PTEP

Prog. Theor. Exp. Phys. **2022** 063B04(22 pages)
DOI: 10.1093/ptep/ptac075

Curved domain-wall fermions

Shoto Aoki* and Hidenori Fukaya*

Department of Physics, Osaka University, Toyonaka, Osaka 560-0043, Japan
*E-mail: saoki@hetmail.phys.sci.osaka-u.ac.jp; hfukaya@het.phys.sci.osaka-u.ac.jp

Received March 9, 2022; Accepted April 28, 2022; Published April 30, 2022

We consider fermion systems on a square lattice with a mass term having a curved domain-wall. Like conventional flat domain-wall fermions, massless and chiral edge states appear on the wall. In the cases of S^1 and S^2 domain-walls embedded into flat hypercubic lattices, we find that these edge modes feel gravity through the induced spin or spin^c connections. The gravitational effect is encoded in the Dirac eigenvalue spectrum as a gap from zero. In the standard continuum extrapolation of the square lattice, we find good agreement with the analytic prediction in the continuum theory. We also find that the rotational symmetry of the edge modes is automatically recovered in the continuum limit. Subject Index B38

1. Introduction

Lattice gauge theory provides a nonperturbative regularization of quantum field theory. In the standard formulation of quantum chromodynamics (QCD), we consider a 4D square lattice with periodic boundary conditions, whose continuum limit is supposed to be a flat torus. Since the degrees of freedom become finite in this regularization, the QCD partition function is expressed by a mathematically well defined integral, which allows a nonperturbative first-principles computation of hadronic processes using numerical simulations.

In contrast to the remarkable success of lattice QCD on a flat Euclidean spacetime, it is not straightforward to formulate a lattice field theory with a gravitational background. Unlike the standard gauge field that is just put as a link variable on a fixed square lattice, the nontrivial metric or vielbein needs some deformation of the lattice itself. In order to systematically achieve such a deformation, previous works [1–7] employed triangular lattices, which correspond to the triangulation of manifolds known in mathematics. They tried to represent dynamical or non-dynamical gravity by changing the lengths and/or angles of the link variables.

One of the problems in such triangular lattice approaches is an ambiguity in taking the continuum limit. On the standard flat square lattice, only one parameter, lattice spacing a (or equivalently gauge coupling), is enough to tune for approaching the continuum limit. It is known that the rotational symmetry (or Lorentz invariance after the Wick rotation) is automatically recovered in that limit if the lattice action respects a discrete subgroup symmetry of it. On the other hand, there is no such simple and unique way for making a finer triangular lattice from a given triangular lattice. It was reported in Ref. [8] that some counterterms are required to recover the rotational symmetry of spherical manifolds.

In this work, we attempt to formulate fermion systems with a nontrivial gravitational background put on a square lattice. In mathematics, it is known that any Riemannian manifold can be isometrically embedded into a sufficiently higher-dimensional Euclidean space [9,10]. If we regularize this higher-dimensional flat space by a square lattice and localize the fermion field

Funded by SCOAP[3]

on the embedded submanifold, the fermion would feel gravity through the spin connection induced by the embedding. Since the total system is given by a flat square lattice, the continuum limit is naturally taken by reducing the lattice spacing, in just the same way as in the standard lattice gauge theory. If the action respects the symmetry under right-angle rotations of the whole system, it is also natural to assume that the rotational symmetry, as well as that of the embedded manifold if it exists, will be automatically recovered in this simple continuum limit.

It is well known in the so-called domain-wall fermion formulation [11–15] that edge-localized states appear on the codimension-one subspace. Moreover, these modes are massless and chiral when the domain-wall is of even dimensions. In lattice QCD, the edge-localized modes are regarded as quarks, and their effective Dirac operator satisfies the Ginsparg–Wilson relation [16] in the infinite limit of the extra dimension, with which one has an exact chiral symmetry on a lattice [17]. With the Dirac operator satisfying the Ginsparg–Wilson relation, the Atiyah–Singer index can be defined even with finite lattice spacings [18]. Recently, the Atiyah–Patodi–Singer index on a manifold with boundaries was reformulated using the domain-wall fermions in continuum theory [19–21], which was extended to the lattice gauge theory [22]. However, as far as we know, the previous works were limited to the cases where the domain-wall is a flat Euclidean space.

In the continuum theory, localized states at the curved subspace have been actively studied. Historically, a free non-relativistic system bounded on a submanifold was first considered in Refs. [23,24] and then they extended the work to the case with an external gauge field in Refs. [25,26]. Furthermore, a similar study was done for the relativistic Dirac field in Refs. [27–31]. These studies pointed out that a geometric potential or a nontrivial spin connection is induced in the effective theory on the surface, and such potentials were experimentally discovered in Refs. [32,33]. Topological insulators having a curved surface or bubbles inside were also considered. In Refs. [34–37], they found that the edge-localized modes appearing on the spherical surface feel gravity through the nontrivial connection. In a relativistic framework, the curved domain-wall was studied in the context of anomaly inflow [12]. For example, it was shown in Ref. [38] that there exists a gravitational anomaly [6,39] in a 3D Kähler–Dirac fermion system and its anomaly is canceled by a contribution from the curved domain-wall.

In this work, we consider the embedding of a circle S^1 as a domain-wall into a 2D Euclidean flat lattice, as well as of a sphere S^2 domain-wall put on a 3D square lattice. On each domain-wall, we find massless states localized at the curved domain-wall, and the Dirac eigenvalue spectrum shows a gravitational effect through the induced spin connection on the wall. A preliminary result has already been presented in Ref. [40].

The rest of the paper is organized as follows. In Sect. 2, we propose a fermion system with a general curved domain-wall mass on a general spin Riemannian manifold. We discuss in continuum theory how the edge modes emerge at the domain-wall and how the induced spin connection is detected from the Dirac operator. In Sects. 3 and 4, we explicitly solve the eigenproblem of the edge modes in the 2D system with an S^1 domain-wall, as well as an S^2 embedded in three dimensions. We compare the numerical lattice results and those in continuum and estimate the finite-volume corrections. Special focus is placed

on the recovery of the rotational symmetry. Finally, we give a summary and discussion in Sect. 5.

2. Curved manifold embedded into Euclidean space

It was shown by Nash [9,10] that any Riemannian manifold can be isometrically embedded into a sufficiently higher-dimensional flat Euclidean space. Conversely, if we have an embedding function of a manifold into a Euclidean space its metric is uniquely determined (induced) by the embedding. In this section, we compute the induced metric as well as the associated spin connection by the embedding. We also discuss how the edge-localized modes of the fermion emerge when the embedding is given by a domain-wall mass term.

2.1. *Induced spin connection by embedding*

Let us consider an n-dimensional Riemannian manifold Y with a metric h, which is isometrically embedded into a Euclidean space $\mathbb{R}^m$ with the m-dimensional flat metric δ (the integer m can be taken finite in a range $m \leq \frac{1}{2}(n+2)(n+5)$ [9,10]). Let us denote the embedding function by $x^I(y^1, y^2, \ldots, y^n)$ where $x^{I=1,2,\ldots,m}$ denotes the coordinate on $X = \mathbb{R}^m$ as a function of the coordinate $y^{i=1,2,\ldots,n}$ on Y. Then, the induced metric h is uniquely determined (up to the diffeomorphism on Y) by

$$h_{ab} = \sum_{IJ} \delta_{IJ} \frac{\partial x^I}{\partial y^a} \frac{\partial x^J}{\partial y^b}. \tag{1}$$

If a particle is constrained on the curved manifold Y, it feels gravity by the equivalence principle, through the induced metric h. In continuum theory, this was confirmed in Refs. [23–25] and experimentally realized in Refs. [32,33]. What about relativistic Dirac fermion fields? According to Refs. [27–31], if Y is a spin manifold, its spin connection is also induced by the embedding.

Let us consider a tangent vector space at $p \in Y$. Since p is also a point of $X (= \mathbb{R}^m)$, we can decompose the tangent space $T_p X$ as

$$T_p X \simeq T_p Y \oplus N_p, \tag{2}$$

where N_p is a normal vector space to $T_p Y$. Let $\{e_1, \ldots, e_n\}$ be a vielbein of Y, then we can choose a vielbein of X as

$$\{\underbrace{e_1, \ldots, e_n}_{\text{vielbein of } Y}, \underbrace{e_{n+1}, \ldots, e_m}_{\text{normal vector}}\}, \tag{3}$$

where $e_I = e_I^{\ J} \frac{\partial}{\partial x^J}$. The component $e_I^{\ J}$ is determined as the following. On Y, the vector $\frac{\partial}{\partial y^a}$ is written as

$$\frac{\partial}{\partial y^a} = \sum_{I=1}^{m} \frac{\partial x^I}{\partial y^a} \frac{\partial}{\partial x^I}. \tag{4}$$

We can regard $\left(\frac{\partial x^I}{\partial y^a}\right)$ as an $m \times n$ matrix with the rank n to obtain the basis transformation

$$\left(\frac{\partial}{\partial y^1}, \dots, \frac{\partial}{\partial y^n}, \frac{\partial}{\partial x^{n+1}}, \dots, \frac{\partial}{\partial x^m}\right)$$
$$= \left(\frac{\partial}{\partial x^1}, \dots, \frac{\partial}{\partial x^n}, \frac{\partial}{\partial x^{n+1}}, \cdots, \frac{\partial}{\partial x^m}\right) \left(\begin{array}{ccc|ccc} \frac{\partial x^1}{\partial y^1} & \cdots & \frac{\partial x^1}{\partial y^n} & & & \\ \vdots & \ddots & \vdots & & & \\ \frac{\partial x^n}{\partial y^1} & \cdots & \frac{\partial x^n}{\partial y^n} & & & \\ \hline \frac{\partial x^{n+1}}{\partial y^1} & \cdots & \frac{\partial x^{n+1}}{\partial y^n} & 1 & & \\ \vdots & \ddots & \vdots & & \ddots & \\ \frac{\partial x^m}{\partial y^1} & \cdots & \frac{\partial x^m}{\partial y^n} & & & 1 \end{array}\right). \tag{5}$$

The vielbein can be obtained by Gram–Schmidt orthonormalization:

$$\begin{aligned} e_1 &= \frac{e_1'}{\| e_1' \|}, \quad \left(e_1' = \frac{\partial}{\partial y^1}\right) \\ e_2 &= \frac{e_2'}{\| e_2' \|}, \quad \left(e_2' = \frac{\partial}{\partial y^2} - \delta\left(e_1, \frac{\partial}{\partial y^2}\right) e_1\right) \\ e_3 &= \cdots, \end{aligned} \tag{6}$$

where $\| v \| = \sqrt{\delta(v, v)}$ for vector fields v on X.

Although X is a flat Euclidean space, the above choice of the vielbein makes the Levi–Civita and spin connections look nontrivial. From the torsionless condition and vielbein postulate, we uniquely obtain the Christoffel symbol:

$$\Gamma^I_{JK} = \frac{1}{2} g^{IA} \left\{ \frac{\partial g_{AJ}}{\partial x^K} + \frac{\partial g_{AK}}{\partial x^J} - \frac{\partial g_{JK}}{\partial x^A} \right\}, \; g^{IJ} = \sum_K e^I_K e^J_K, \tag{7}$$

as well as the spin connection (when Y is a spin manifold):

$$\omega_K = \frac{1}{4} \sum_{KJ} \omega_{IJ,K} \gamma^I \gamma^J, \; \omega^I_{J,K} = -\frac{1}{2} \left(C^I_{J,K} + C^J_{K,I} - C^K_{I,J} \right), \tag{8}$$

where $C^K_{I,J}$ is defined by the commutator $[e_I, e_J] = e_K C^K_{I,J}$ and is written as

$$C^K_{I,J} = g^{NM} e_K^N \left(e_I^L \frac{\partial e_J^M}{\partial x^L} - e_J^L \frac{\partial e_I^M}{\partial x^L} \right). \tag{9}$$

The spin connection on Y can be identified by simply collecting those having indices in $\{1, \dots, n\}$:

$$\omega_c = \frac{1}{4} \sum \omega_{ab,c} \gamma^a \gamma^b. \tag{10}$$

Note that the above connections give zero curvature everywhere on X.

Next, we consider a domain-wall fermion system where the mass term flips its sign on a codimension-one manifold Y embedded into $X = \mathbb{R}^{n+1}$. Let $f : X \to \mathbb{R}$ be a smooth function such that $f^{-1}(0) \neq \emptyset$ and $df|_p \neq 0$ for all $p \in f^{-1}(0)$. Then $Y := f^{-1}(0)$ is a hypersurface in X and an n-dimensional smooth manifold by the preimage theorem. Y can be regarded as a domain-wall dividing X into the $f > 0$ and $f < 0$ regions. We can take a vielbein $\{e_1, \dots, e_{n+1}\}$ as Eq. (3). Since $\{e_1, \dots, e_n\}$ are tangent vectors of Y,

$$e_a(f) = e^I_a \frac{\partial f}{\partial x^I} = 0 \tag{11}$$

or equivalently we have

$$e_{n+1} = \frac{1}{\| \operatorname{grad}(f) \|} \operatorname{grad}(f), \tag{12}$$

where $\operatorname{grad}(f) = \sum_I g^{IJ} \frac{\partial f}{\partial x^I} \frac{\partial}{\partial x^J}$. The Dirac operator on X is

$$\begin{aligned} \not{D} + m\epsilon = \gamma^a \left(e_a + \frac{1}{4} \sum_{bc} \omega_{bc,a} \gamma^b \gamma^c + \frac{1}{2} \sum_b \omega_{b\ n+1,a} \gamma^b \gamma^{n+1} \right) \\ + \gamma^{n+1} \left(e_{n+1} + \frac{1}{4} \sum_{bc} \omega_{bc,n+1} \gamma^b \gamma^c + \frac{1}{2} \sum_b \omega_{b\ n+1,n+1} \gamma^b \gamma^{n+1} \right) + m\epsilon, \end{aligned} \tag{13}$$

where $\epsilon = \operatorname{sign}(f)$ is a step function.

Let us decompose the above Dirac operator into the one on Y and that in the normal direction. First, note that we can take $\omega^b{}_{c,n+1} = \omega_{bc,n+1} = 0$ by a local $spin(n)$ rotation. Let us denote the coordinate in the normal direction by t. Then $\omega_{bc,\,n+1}$ is absent in the transformed Dirac operator

$$\not{D} \to L^{-1}(y,t) \not{D} L(y,t), \tag{14}$$

$$L(y,t) = P \exp \left[-\frac{1}{4} \sum_{bc} \gamma^b \gamma^c \int_0^t dt' \omega_{bc,n+1}(y,t') \right], \tag{15}$$

where P denotes the path-ordered product.

Next, we compute $\omega^b{}_{n+1,n+1} = \omega_{b\ n+1,n+1}$. According to Eq. (8), it is enough to obtain $C^{n+1}_{b,n+1}$. Using the commutator

$$[e_b, e_{n+1}] = C^c_{b,n+1} e_c + C^{n+1}_{b,n+1} e_{n+1}, \tag{16}$$

and $df(e_{n+1}) = \delta(\operatorname{grad}(f), e_{n+1}) = \|\operatorname{grad}(f)\|$, we have a relation

$$\begin{aligned} 0 &= ddf(e_b, e_{n+1}) = e_b df(e_{n+1}) - e_{n+1} df(e_b) - df([e_b, e_{n+1}]) \\ &= e_b (\| \operatorname{grad}(f) \|) - C^{n+1}_{b,n+1} \| \operatorname{grad}(f) \|. \end{aligned} \tag{17}$$

Since $\|\operatorname{grad}(f)\|$ is nonzero around Y, we obtain

$$\begin{aligned} \omega^b{}_{n+1,n+1} &= -\frac{1}{2} \left(C^b_{n+1,n+1} + C^{n+1}_{n+1,b} - C^{n+1}_{b,n+1} \right) = C^{n+1}_{b,n+1} \\ &= \frac{1}{\| \operatorname{grad}(f) \|} e_b (\| \operatorname{grad}(f) \|) = \frac{1}{2} e_b \left(\log \left(g^{IJ} \frac{\partial f}{\partial x^I} \frac{\partial f}{\partial x^J} \right) \right). \end{aligned} \tag{18}$$

Finally, let us denote the remaining connection $\omega^b{}_{n+1,a}$ by $\omega^b{}_{n+1,a} = -h_{ab}$, which is known as the second fundamental form or shape operator. Since $\omega^a{}_{n+1,b} - \omega^b{}_{n+1,a} = C^{n+1}_{a,b} = 0$, h_{ab} is symmetric: $h_{ab} = h_{ba}$. Now the Dirac operator becomes

$$\begin{aligned} \not{D} + m\epsilon &= \gamma^a \left(\tilde{\nabla}_{e_a} \right) + \frac{1}{2} \sum_{ab} (-h_{ab}) \gamma^a \gamma^b \gamma^{n+1} \\ &\quad + \gamma^{n+1} \left(e_{n+1} + \frac{1}{4} \sum_b e_b \left(\log \left(g^{IJ} \frac{\partial f}{\partial x^I} \frac{\partial f}{\partial x^J} \right) \right) \gamma^b \gamma^{n+1} \right) + m\epsilon \\ &= \gamma^a \left(\tilde{\nabla}_{e_a} \right) + \gamma^{n+1} \left(e_{n+1} - \frac{1}{2} \operatorname{tr} h + \frac{1}{4} e_a \left(\log \left(g^{IJ} \frac{\partial f}{\partial x^I} \frac{\partial f}{\partial x^J} \right) \right) \gamma^a \gamma^{n+1} \right) + m\epsilon. \end{aligned} \tag{19}$$

Here $\frac{1}{n} \operatorname{tr} h = \frac{1}{n} \sum_a h_{aa}$ corresponds to the mean curvature of the n-dimensional Riemannian submanifold Y. This expression is consistent with the previous works [27–31].

In order to solve the Dirac equation, it may be convenient to perform a rescaling transformation $\psi = \left(g^{IJ}\frac{\partial f}{\partial x^I}\frac{\partial f}{\partial x^J}\right)^{\frac{1}{4}}\psi'$. On ψ', the Dirac operator acts as

$$\not{D}' + m\epsilon = \gamma^a\left(e_a + \frac{1}{4}\sum_{bc}\omega_{bc,a}\gamma^b\gamma^c\right) + \gamma^{n+1}\left(e_{n+1} - \frac{1}{2}\mathrm{tr}\,h + \frac{1}{4}e_{n+1}\left(\log\left(g^{IJ}\frac{\partial f}{\partial x^I}\frac{\partial f}{\partial x^J}\right)\right)\right) + m\epsilon. \tag{20}$$

The first term corresponds to the massless Dirac operator on Y, where we can find the induced gravity effect as a nontrivial spin connection. This form suggests the existence of massless edge modes no matter how Y is curved, when we find a function of the normal coordinate t on which the second and third terms of the operator give zero.

As a final remark in this subsection, we note that the above result for the Dirac operator is valid only locally, although the original coordinates and operator are defined globally on $X = \mathbb{R}^m$. To obtain the global solution of the Dirac equation, we need to separately find the solutions on the open patches covering X and check the consistency conditions on them. As will be discussed below, the Berry phase of the spinor field may help to simplify this issue. We also note that when Y is a closed manifold the spin structure of Y must belong to the trivial element of the spin bordism group.

2.2. *Edge-localized modes on the domain-walls*

In this subsection, let us examine the existence of the edge-localized modes formally solving the Dirac equation. Let Y be an n-dimensional submanifold of $X = \mathbb{R}^{n+1}$ embedded by a function $f : X \to \mathbb{R}$. We can express Dirac's gamma matrices by

$$\gamma^a = -\sigma_2 \otimes \tilde{\gamma}^a,\ \gamma^{n+1} = \sigma_1 \otimes 1,\ \bar{\gamma} = \sigma_3 \otimes 1, \tag{21}$$

where $\tilde{\gamma}^a$ $(a = 1, \ldots, n)$ are the $2^{[n/2]} \times 2^{[n/2]}$ gamma matrices ($[\alpha]$ denotes the Gauss symbol or the integer part of α) that satisfy the Clifford algebra in n dimensions, and $\sigma_{1,2,3}$ are the Pauli matrices. When n is even, the above gamma matrices are not in the irreducible representation and the Pauli matrices can be interpreted as the operators on the two-flavor space. In general, the massive Dirac operator is a complex operator in odd dimensions. In order to make a well defined eigenvalue problem of a Hermitian operator, we introduce these two flavors of the spinor fields[1]. Since $\bar{\gamma}$ anti-commutes with any other γ, we call it the "chirality" operator on X. Unlike the standard flat domain-wall fermion, however, the edge-localized modes are eigenstates of another "chirality" operator, different from $\bar{\gamma}$, as is discussed below.

Expressing the Dirac spinor on X by

$$\psi = \begin{pmatrix}\chi_1\\ \chi_2\end{pmatrix}, \tag{22}$$

let us solve the eigenproblem of the Hermitian Dirac operator on ψ:

$$H = \bar{\gamma}(\not{D} + \epsilon m). \tag{23}$$

Around $p \in Y$, we can set a chart $(y^1, \ldots, y^n, t)$ and its associated frame, where $(y^1, \ldots, y^n)$ denotes the coordinate along Y and t is that in the direction of the normal vector e_{n+1}. Here $t = 0$ denotes where Y is located. On this chart, $\epsilon = \mathrm{sign}(t)$. Let $\psi = \left(g^{IJ}\frac{\partial f}{\partial x^I}\frac{\partial f}{\partial x^J}\right)^{\frac{1}{4}}\psi'$. On ψ', the

[1] In Appendix A we consider the one-flavor "chiral" case where the Dirac operator is non-Hermitian.

Dirac operator acts as

$$H' = \bar{\gamma}(\not{D}' + \epsilon m) = \begin{pmatrix} \epsilon m & i\tilde{\not{D}} + \frac{\partial}{\partial t} + F \\ i\tilde{\not{D}} - \frac{\partial}{\partial t} - F & -\epsilon m \end{pmatrix}, \tag{24}$$

where $F = -\frac{1}{2}\mathrm{tr}\, h + \frac{1}{4}\frac{\partial}{\partial t}\left(\log\left(g^{IJ}\frac{\partial f}{\partial x^I}\frac{\partial f}{\partial x^J}\right)\right)$ is a function of $(y^1, \ldots, y^n, t)$ in general and $i\tilde{\not{D}} = \tilde{\gamma}^a\tilde{\nabla}_a$ is the Dirac operator on Y.

Let us consider a solution with an eigenvalue much smaller than m. In the large-m limit, the following part of the operator H' must vanish separately:

$$H'_{\mathrm{normal}} = i\sigma_2\left(\frac{\partial}{\partial t} + F + \sigma_1 m\epsilon\right) \otimes 1, \tag{25}$$

which requires the solution to have the form

$$\psi' = e^{-m|t|}\left[\exp\left(-\int_0^t dt' F(y,t')\right)\begin{pmatrix}\chi(y)\\ \chi(y)\end{pmatrix} + \mathcal{O}(t)\right]. \tag{26}$$

If we take $\chi(y)$ to be an eigenstate of $i\tilde{\not{D}}|_{t=0}$ with the eigenvalue λ, we obtain the edge-localized mode of H in the $m \to \infty$ limit by

$$\psi = \left(g^{IJ}\frac{\partial f}{\partial x^I}\frac{\partial f}{\partial x^J}\right)^{\frac{1}{4}} e^{-m|t|}\exp(-\int_0^t dt' F(y,t'))\begin{pmatrix}\chi(y)\\ \chi(y)\end{pmatrix}, \tag{27}$$

which has a negative eigenvalue for the "chirality" operator $\gamma^{n+1} = \sigma_1 \otimes 1$ and the eigenvalue λ of the massless n-dimensional operator: $i\tilde{\not{D}}|_{t=0}\chi(y) = \lambda\chi(y)$. These modes feel gravity through the induced spin connection in the effective Dirac operator on Y.

Finally, let us evaluate the leading-order contribution of the finite $1/m$ corrections. From the above solution, we have

$$(H-\lambda)\psi = \left(g^{IJ}\frac{\partial f}{\partial x^I}\frac{\partial f}{\partial x^J}\right)^{\frac{1}{4}} e^{-m|t|}e^{-\int_0^t dt' F(y,t')}\underbrace{\left(-\int_0^t dt'\gamma^a e_a(F(y,t'))\right)}_{\mathcal{O}(t)}\begin{pmatrix}\chi(y)\\ \chi(y)\end{pmatrix}. \tag{28}$$

In the limit of $m \gg |F(y,t)|$, we can estimate the magnitude of the residual error as

$$\| (H-\lambda)\psi \| \le \frac{C}{m}, \tag{29}$$

where $\|*\|$ denotes the norm of the Dirac spinor on X and C is a positive number independent of m. Therefore, ψ becomes an eigenstate of H when m is large enough.

3. S^1 domain-wall in 2D flat space

In this section, we embed a 1D sphere S^1 as a domain-wall into the flat 2D space. This situation is the simplest case to which the argument of Sect. 2.2 applies.

3.1. *Continuum analysis*

The Hermitian Dirac operator (23) in this case is

$$H = \sigma_3\left(\sigma_1\frac{\partial}{\partial x} + \sigma_2\frac{\partial}{\partial y} + m\epsilon\right) = \begin{pmatrix} m\epsilon & e^{-i\theta}\left(\frac{\partial}{\partial r} - \frac{i}{r}\frac{\partial}{\partial\theta}\right) \\ -e^{i\theta}\left(\frac{\partial}{\partial r} + \frac{i}{r}\frac{\partial}{\partial\theta}\right) & -m\epsilon \end{pmatrix}, \tag{30}$$

in the continuum Euclidean space $\mathbb{R}^2$, where an S^1 domain-wall with radius r_0 is put by the sign function $\epsilon = \mathrm{sign}(r - r_0)$. We take the polar coordinates (r, θ) so that the radial direction is equal to the normal direction to the S^2 domain-wall. Here ψ is a two-component spinor on $\mathbb{R}^2$.

In Eq. (30), the sigma matrix in the normal direction and that in the tangent direction are

$$\sigma_r = \sigma_1 \cos\theta + \sigma_2 \sin\theta, \ \ \sigma_\theta = \sigma_2 \cos\theta - \sigma_1 \sin\theta. \tag{31}$$

By a local *spin*(2) gauge transformation, we can take a frame where they are universally given by $\sigma_r \to e^{-i\frac{\theta}{2}\sigma_3}\sigma_r e^{i\frac{\theta}{2}\sigma_3} = \sigma_1$ and $\sigma_\theta \to e^{-i\frac{\theta}{2}\sigma_3}\sigma_\theta e^{i\frac{\theta}{2}\sigma_3} = \sigma_2$, respectively. However, this transformation spoils the original periodic property of the spinor $\psi(r, \theta + 2\pi) = \psi(r, \theta)$. As discussed in the previous section, this simply reflects the fact that the frame can be taken only locally and careful gluing of them is required to give a consistent result. Here we avoid this issue by a further $U(1)$ transformation $e^{-i\frac{\theta}{2}}$, which produces a Berry connection (or *spin*^{c}(1) connection in mathematics). Specifically, we transform the spinor as $\psi \to \psi' = e^{i\frac{\theta}{2}\sigma_3}e^{-i\frac{\theta}{2}}\psi$ keeping its periodicity to obtain the transformed Dirac operator

$$\begin{aligned} H' &= e^{i\frac{\theta}{2}\sigma_3}e^{-i\frac{\theta}{2}} H e^{-i\frac{\theta}{2}\sigma_3}e^{+i\frac{\theta}{2}} \\ &= \sigma_3 \left(\sigma_1 \left(\frac{\partial}{\partial r} + \frac{1}{2r} \right) + \sigma_2 \frac{1}{r} \left(\frac{\partial}{\partial \theta} + i\frac{1}{2} \right) + m\epsilon \right), \end{aligned} \tag{32}$$

which operates on the periodic spinor.

The explicit form of the eigenfunction with the the eigenvalue $-m < E < m$ of H' is given by

$$(\psi^{E,j})' = \begin{cases} A \begin{pmatrix} \sqrt{m^2 - E^2} I_{j-\frac{1}{2}}(\sqrt{m^2 - E^2} r) e^{i(j-\frac{1}{2})\theta} \\ (m+E) I_{j+\frac{1}{2}}(\sqrt{m^2 - E^2} r) e^{i(j-\frac{1}{2})\theta} \end{pmatrix} & (r < r_0) \\ B \begin{pmatrix} (m+E) K_{j-\frac{1}{2}}(\sqrt{m^2 - E^2} r) e^{i(j-\frac{1}{2})\theta} \\ \sqrt{m^2 - E^2} K_{j+\frac{1}{2}}(\sqrt{m^2 - E^2} r) e^{i(j-\frac{1}{2})\theta} \end{pmatrix} & (r > r_0) \end{cases}, \tag{33}$$

where j takes a half-integer value $j = \pm\frac{1}{2}, \pm\frac{3}{2}, \ldots$. Here I_n and K_n are the modified Bessel functions. From their exponentially decaying asymptotic form, this eigenfunction represents an edge-localized mode at $r = r_0$. From the continuity at $r = r_0$, the coefficients A and B are determined (with the normalization condition) and we obtain a nontrivial eigenvalue condition:

$$\frac{I_{j-\frac{1}{2}}}{I_{j+\frac{1}{2}}} \frac{K_{j+\frac{1}{2}}}{K_{j-\frac{1}{2}}}(\sqrt{m^2 - E^2} r_0) = \frac{m+E}{m-E}. \tag{34}$$

In the large-mass limit or $m \gg E$, the eigenvalue converges to

$$E \simeq \frac{j}{r_0} \ \left(j = \pm\frac{1}{2}, \pm\frac{3}{2}, \ldots \right). \tag{35}$$

The normalized eigenfunction in that limit is also simplified as[2]

$$\left(\psi^{E,j}_{\text{edge}}\right)' \simeq \sqrt{\frac{m}{4\pi r}} e^{-m|r-r_0|} \begin{pmatrix} e^{i(j-\frac{1}{2})\theta} \\ e^{i(j-\frac{1}{2})\theta} \end{pmatrix}, \tag{36}$$

which is chiral with respect to a gamma matrix σ_1 facing the normal direction to the domain-wall with the eigenvalue $+1$. σ_1 corresponds to σ_r in the original frame of $\mathbb{R}^2$.

In order to identify the induced gravity effect, let us solve the eigenproblem again taking the $m \to \infty$ limit first. To obtain the finite eigenvalue in this limit, the solution must have the form

$$\psi'_{\text{edge}} = \sqrt{\frac{m}{4\pi r}} e^{-m|r-r_0|} \begin{pmatrix} 1 \\ 1 \end{pmatrix} \chi'(\theta), \tag{37}$$

to cancel the m dependence of the operator. On this edge mode, the Dirac operator effectively acts as

$$-i\frac{1}{r_0}\left(\frac{\partial}{\partial\theta} + i\frac{1}{2} \right), \tag{38}$$

[2]This approximation is only valid at $r \sim r_0$.

where we have used $\sigma_1 = 1$.

Here, the second term $1/2r_0$ can be identified as the induced spin^c connection. It is now obvious from the Fourier transformation of $\chi'(\theta) \to \exp(in\theta)$, $n \in \mathbb{Z}$, that the eigenvalue takes a half-integer $j = n + 1/2$ multiplied by $1/r_0$. The gap in the eigenvalue spectrum seen in Eq. (35) opens due to this gravitational effect.

One can locally cancel the gravitational effect or the connection term by a $U(1)$ transformation $\chi' \to \chi = e^{i\theta/2}\chi'$. However, the global effect of the curved S^1 remains as the anti-periodic boundary condition of χ, leaving the eigenvalue spectrum including the gap unchanged. In mathematics, the anti-periodic χ field is more natural on S^1 in the sense that it belongs to a trivial element in the spin bordism group. The induced spin^c connection naturally describes how the anti-periodicity emerges in the effective low-energy theory of edge modes, for which the total original system is made periodic.

3.2. *Lattice analysis*

Let us discretize the Dirac operator (30) on a 2D square lattice $(\mathbb{Z}/N\mathbb{Z})^2$. When we take the lattice size $L = 1$, the lattice spacing is simply given by $a = 1/N$. We represent $\hat{x} = x/a$ and $\hat{y} = y/a$ as the coordinates of $(\mathbb{Z}/N\mathbb{Z})^2$ in the range $0 \le \hat{x}, \hat{y} \le N - 1$ and we assume the periodic boundary condition $\hat{x} = 0 \sim N$, $\hat{y} = 0 \sim N$. Denoting the difference operators by $(\nabla_1 \psi)_{(\hat{x},\hat{y})} = \psi_{(\hat{x}+1,\hat{y})} - \psi_{(\hat{x},\hat{y})}$ and $(\nabla_1^\dagger \psi)_{(\hat{x},\hat{y})} = \psi_{(\hat{x}-1,\hat{y})} - \psi_{(\hat{x},\hat{y})}$ and those in the $\hat{y}$ in the same manner, we have the lattice version of the domain-wall Dirac operator

$$H = \frac{1}{a}\sigma_3 \left(\sum_{i=1,2} \left[\sigma_i \frac{\nabla_i - \nabla_i^\dagger}{2} + \frac{1}{2}\nabla_i \nabla_i^\dagger \right] + \epsilon_A am \right), \tag{39}$$

where we have introduced the Wilson term (the second term in the square brackets) with the standard choice of the coefficient $w = 1$. We assign the domain-wall mass by a step function

$$\epsilon_A(\hat{x}, \hat{y}) = \begin{cases} -1 & ((\hat{x}, \hat{y}) \in A) \\ 1 & ((\hat{x}, \hat{y}) \notin A) \end{cases}. \tag{40}$$

The region A inside the circle is defined by

$$A = \left\{ (\hat{x}, \hat{y}) \in (\mathbb{Z}/N\mathbb{Z})^2 \mid \left(\hat{x} - \frac{N-1}{2}\right)^2 + \left(\hat{y} - \frac{N-1}{2}\right)^2 < (\hat{r}_0)^2 \right\}, \tag{41}$$

where $\hat{r}_0 = r_0/a$ is the radius of the S^1 domain-wall in the lattice units and $(\frac{N-1}{2}, \frac{N-1}{2})$ is the center of the circle. Note that $\frac{N-1}{2}$ needs not to be an integer. In fact, we take N even for the reason explained below.

Since the domain-wall is curved, the chirality operator is position-dependent. Let us translate $\hat{x} - \frac{N-1}{2} \to \hat{x}$ and $\hat{y} - \frac{N-1}{2} \to \hat{y}$ so that the center of the circle is located at (0,0), and $\hat{x}$ (resp. $\hat{y}$) takes a half-integer when N is even. Then, we can define the chirality operator on the lattice by

$$\gamma_{\text{normal}} := \sigma_1 \frac{\hat{x}}{\hat{r}} + \sigma_2 \frac{\hat{y}}{\hat{r}} \tag{42}$$

where $\hat{r} = \sqrt{\hat{x}^2 + \hat{y}^2}$. This operator is well defined only when N is even.

We solve the eigenvalue problem of Eq. (39) numerically and compute the expectation value of the chirality of each eigenstate. We plot the eigenvalues in Fig. 1 and represent their chirality by gradation of the symbol. Here we set the lattice size $N = 20$, the radius of the circle domain-wall $\hat{r}_0 = r_0/a = 5$, and the fermion mass $ma = 0.7$. The circle symbols denote the lattice data

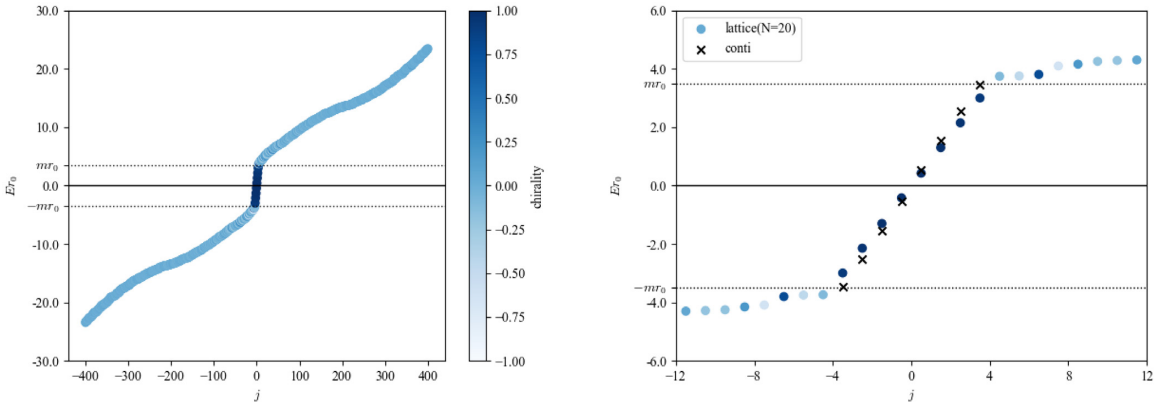

Fig. 1. The eigenvalue spectrum of the domain-wall Dirac operator at $ma = 0.7$, $\hat{r}_0 = r_0/a = 5$, and $N = 20$. Circles denote the lattice data and crosses between $-mr_0$ and mr_0 represent the continuum counterpart. The gradation of the symbols represents chirality. The left panel shows the whole spectrum and the right panel focuses on the near-zero eigenvalues.

and crosses represent their continuum limit. Here we label the eigenvalues with the half-integer j, expecting them to represent the eigenstates

$$\cdots \le E_{-\frac{3}{2}} \le E_{-\frac{1}{2}} \le 0 \le E_{\frac{1}{2}} \le E_{\frac{3}{2}} \le \cdots . \tag{43}$$

The eigenvalues of the near-zero modes, whose absolute value is less than m (indicated by the dotted lines), agree well with their continuum counterparts. The gap from zero, as the gravitational effect, is clearly seen. Moreover, they have positive chirality as expected. These states are localized at the curved domain-wall as shown in Fig. 2 where the amplitude of the $E_{\frac{1}{2}} = 0.4235/r_0$ eigenvector, which has the chirality 0.9902, is plotted.

Let us discuss the systematics due to the finite lattice spacings. In Fig. 3, we plot the relative deviation of $E_{\frac{1}{2}}$ with three finite masses $m = 10/L$, $14/L$, $20/L$ from the continuum result E_{conti},

$$\text{error} = (E - E_{\text{conti}})/E_{\text{conti}}, \tag{44}$$

as a function of the lattice spacing $a = 1/N$. Although some oscillation is visible in the left panel (which is reduced after three-point binning in the right panel), the data show a linear dependence on the lattice spacing a to the continuum limit. We also find that the chirality expectation value approaches the continuum value 0.9966, as presented in Fig. 4. Note that the edge mode is not perfectly chiral even in the continuum theory, due to the finite values of m and r_0.

Next, we discuss the finite-volume effects. In the numerical analysis on the lattice, we assign the periodic boundary condition in every direction with a finite size of L. In Fig. 5 we plot the eigenvalue $r_0 E_{\frac{1}{2}}$ as a function of the lattice size $N = L/a$ with fixed values of $r_0 = 10a$ and $ma = 0.35$. For lattice sizes greater than $N = 40$ or $L = 4r_0$, the finite-volume effect is negligible.

Finally, let us address the recovery of the rotational symmetry. The zigzag behavior of the peaks of the amplitude of the eigenfunction in Fig. 2 reflects the violation of the rotational symmetry on the square lattice. However, we find that the spiky shapes become weaker and weaker when we decrease the lattice spacing. In order to quantify the rotational symmetry violation, we compare the highest and lowest peaks of the amplitude of the eigenfunction with $E_{\frac{1}{2}}$. The local amplitude $(\psi^\dagger\psi)_{(\hat{x},\hat{y})}$ represents the probability distribution of the eigenstate on the $a \times a$ square at the lattice point $(\hat{x}, \hat{y})$. We collect a set of peaks per $\hat{x}$ slices:

$$P = \left\{ \max_{\hat{y}} (\psi^\dagger \psi_{(\hat{x},\hat{y})}) \mid -\hat{r}_0 < \hat{x} < \hat{r}_0 \right\} \tag{45}$$

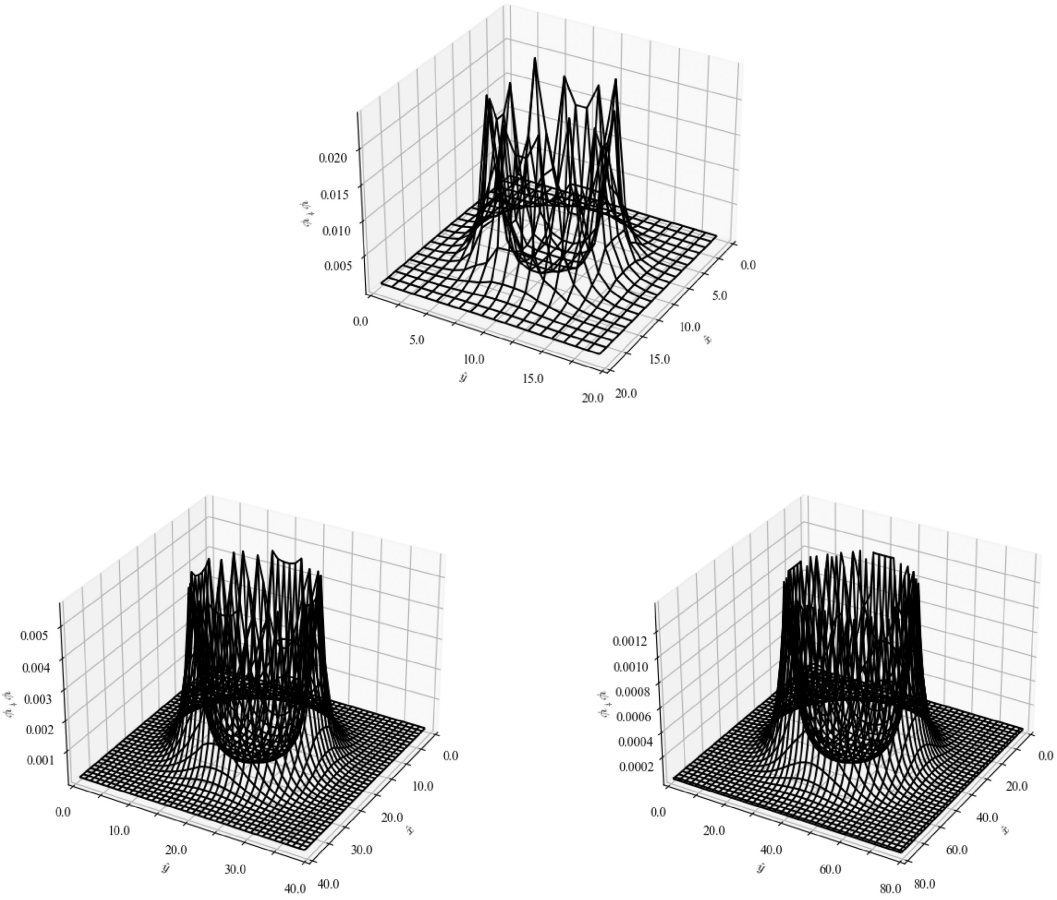

Fig. 2. Top: the amplitude of the eigenfunction with $E_{\frac{1}{2}}$ at the lattice spacing $a = 1/N = L/20$. Bottom left: the same as the top panel but with $a = L/40$. Bottom right: the same but with $a = L/80$.

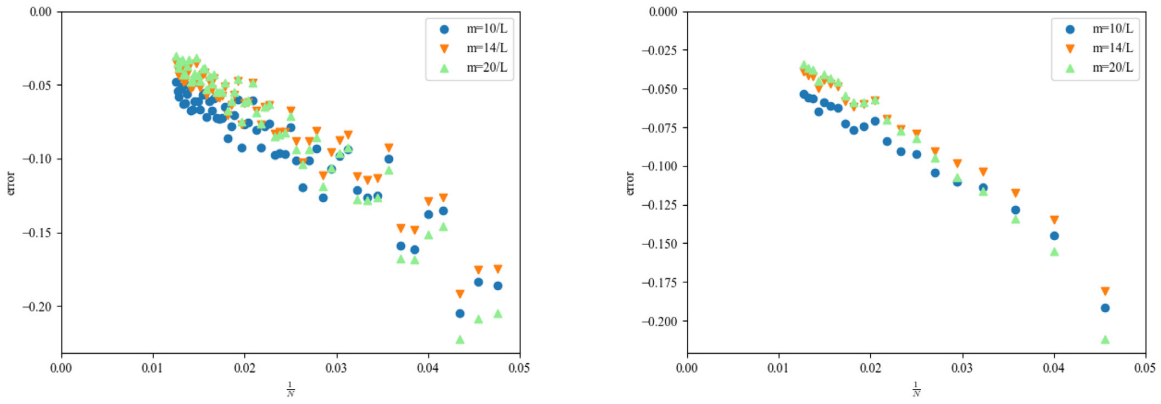

Fig. 3. Left: the relative deviation of the eigenvalue $\left(E_{\frac{1}{2}} - E_{\text{conti}}\right)/E_{\text{conti}}$ is plotted as a function of the lattice spacing $a = \frac{1}{N}$. Right: the same plot as the left panel but with the three neighborhood points averaged.

and take the difference between the maximum and minimum of the set:

$$\Delta_{\text{peak}} = (\max(P) - \min(P))/a^2. \tag{46}$$

We plot Δ_{peak} as a function of the lattice spacing $a = 1/N$ in Fig. 6. Our data indicate automatic

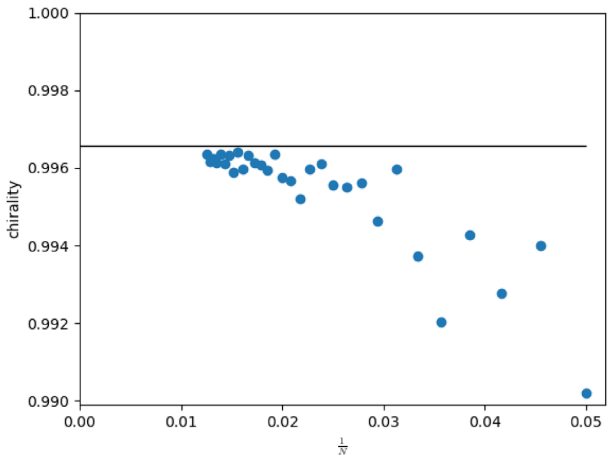

Fig. 4. The chirality of the state with $E_{\frac{1}{2}}$ when $m = 14/L$ and $\hat{r}_0 = L/4$ is plotted as a function of the lattice spacing $a = \frac{1}{N}$. The horizontal line at 0.9966 indicates the continuum value.

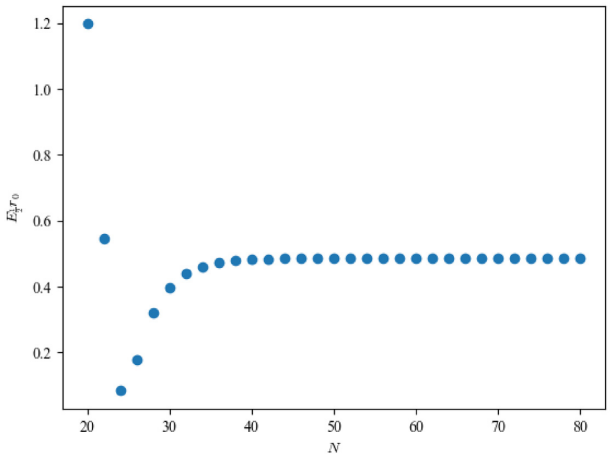

Fig. 5. Finite lattice size N scaling of the eigenvalue $E_{\frac{1}{2}} r_0$ at $ma = 0.35$ and $\hat{r}_0 = 10$.

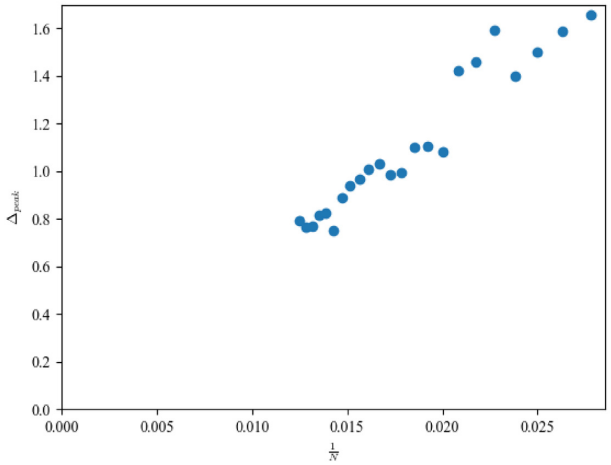

Fig. 6. The rotational symmetry violation measured by the difference between the highest peak and the lowest peak of the amplitude of the eigenfunction with $E_{\frac{1}{2}}$ ($m = 14/L$ and $r_0 = L/4$). See the main text for the details.

recovery of the rotational symmetry, as is naively expected from its recovery of the higher-dimensional square lattice.

4. S^2 domain-wall in 3D flat space

In this section, we embed an S^2 into the 3D Euclidean space as a domain-wall. Here, we locate its center at (0,0,0) and denote its radius by r_0. In general, the massive Dirac operator $D + m$ is a complex operator in three dimensions. In order to make a well defined eigenvalue problem, we introduce two flavors of the spinor fields. One can regard this system as a one-flavor 4D fermion with one direction compactified to an infinitesimal size. In the latter interpretation, the existence of the chiral symmetry is obvious.

4.1. *Continuum analysis*

In continuum theory, our target Hermitian Dirac operator is

$$H = \gamma^5 \left(\sum_{j=1}^{3} \gamma^j \frac{\partial}{\partial x^j} + m\epsilon \right) = \begin{pmatrix} m\epsilon & \sigma^j \partial_j \\ -\sigma^j \partial_j & -m\epsilon \end{pmatrix}, \tag{47}$$

where the gamma matrices are given by a direct product of 2×2 matrices: $\gamma^5 = \sigma_3 \otimes 1,\ \gamma^j = \sigma_1 \otimes \sigma_j$. The former 2×2 matrices can be regarded as an operator on the two-flavor space. The mass parameter is denoted by m and $\epsilon = \mathrm{sign}(r - r_0)$ is a step function. Let us take the standard polar coordinate (r, θ, ϕ) so that the radial direction is equal to the normal direction to the domain-wall, and the remaining θ and ϕ directions are tangent to it. This operator acts on the two flavors of the spinor fields in $\mathbb{R}^3$, or a four-component fermion.

First, let us solve the eigenproblem of Eq. (47) following the general recipe shown in Sect. 2. By a $spin(3) \simeq SU(2)$ rotation,

$$R(\theta, \phi) = \exp(\theta[\gamma^3, \gamma^1]/4) \exp(\phi[\gamma^1, \gamma^2]/4) = 1 \otimes \exp(i\theta\sigma_2/2) \exp(i\phi\sigma_3/2), \tag{48}$$

we can align the gamma matrices in the radial direction to γ^3 and that in the $\theta,\ \phi$ directions to γ^1 and γ^2, respectively. However, this matrix is valid only locally and the same problem arises as in the previous section, in particular on the periodicity with respect to ϕ. Therefore, we perform a further $U(1)$ rotation $\exp(-i\phi/2)$ to obtain the transformed spinor field $\psi' = \exp(-i\phi/2) R(\theta, \phi)\psi$. Then the Hamiltonian is transformed as

$$\begin{aligned} H' &= e^{-i\frac{\phi}{2}} R(\theta, \phi) H R(\theta, \phi)^{-1} e^{i\frac{\phi}{2}} \\ &= \begin{pmatrix} \epsilon m & \sigma_3 \left(\frac{\partial}{\partial r} + \frac{1}{r} + \frac{1}{r}\sigma_3 \mathbb{D}'_{S^2} \right) \\ -\sigma^3 \left(\frac{\partial}{\partial r} + \frac{1}{r} + \frac{1}{r}\sigma^3 \mathbb{D}'_{S^2} \right) & -\epsilon m \end{pmatrix} \end{aligned} \tag{49}$$

and $\mathbb{D}'_{S^2}$ is

$$\mathbb{D}'_{S^2} = \left(\sigma_1 \frac{\partial}{\partial \theta} + \sigma_2 \left(\frac{1}{\sin\theta} \frac{\partial}{\partial \phi} + \frac{i}{2\sin\theta} - \frac{\cos\theta}{2\sin\theta} \sigma_1\sigma_2 \right) \right), \tag{50}$$

where we find nontrivial spin and spin^c connections.

In a similar way to the previous section, the large-m limit requires the edge-localized solution to have the form

$$\psi' = \frac{e^{-m|r-r_0|}}{r} \begin{pmatrix} \chi'(\theta, \phi) \\ \sigma_3 \chi'(\theta, \phi) \end{pmatrix}, \tag{51}$$

which has the positive "chirality" of $\gamma^3 = \begin{pmatrix} 0 & \sigma_3 \\ \sigma_3 & 0 \end{pmatrix}$, or the gamma matrix in the normal direction in the original frame:

$$\gamma_{\text{normal}} := \sum_{i=1}^{3} \frac{x^i}{r} \gamma^i. \tag{52}$$

Here, χ converges to an eigenstate of the massless Dirac operator $\frac{1}{r}\not{D}'_{S^2}\sigma_3|_{r=r_0} = \frac{1}{r_0}\not{D}'_{S^2}\sigma_3$ on the S^2 domain-wall. As explicitly seen in Eq. (50), the edge-localized modes feel gravity through the induced spin and spin^c connections.

According to Ref. [41], $\not{D}'_{S^2}\sigma_3$ is commutative with

$$J'_\pm = \frac{e^{\pm i\phi}}{\sqrt{2}} \left\{ \pm \frac{\partial}{\partial\theta} + i \frac{\cos\theta}{\sin\theta} \left(\frac{\partial}{\partial\phi} + \frac{i}{2} \right) + \frac{1}{2\sin\theta}\sigma_3 \right\}, \; J'_3 = -i\frac{\partial}{\partial\phi} + \frac{1}{2} \tag{53}$$

and a parity operator

$$P\chi(\theta,\phi) = \sigma_1 \chi(\pi - \theta, \phi + \pi). \tag{54}$$

$J'_\pm$ and J'_3 satisfy

$$[J'_+, J'_-] = J'_3, \; [J'_3, J'_\pm] = \pm J'_\pm. \tag{55}$$

Thus the eigenstate of $\not{D}'_{S^2}\sigma_3$ is that of $(J')^2 = J'_+J'_- + J'_-J'_+ + J'_3J'_3$, J'_3, and P. Due to the nontrivial connections, the eigenvalues of $(J')^2$ and J_3 are represented by half-integers by $j(j+1)$ ($j = \frac{1}{2}, \frac{3}{2}, \ldots$); that of J'_3 is denoted as $j_3 = -j, -j+1, \ldots, j-1, j$. The highest eigenfunction with $(j, j_3 = j)$ is obtained from the condition $J'_+\chi'_{j,j_3=j} = 0$ as

$$\chi'_{j,j_3=j,\pm} = (e^{i\phi}\sin\theta)^{j-\frac{1}{2}} \begin{pmatrix} \cos\frac{\theta}{2} \\ \mp\sin\frac{\theta}{2} \end{pmatrix}, \tag{56}$$

which has the eigenvalue $(-1)^{j\pm\frac{1}{2}}$ of P. By a direct substitution, we find that $\chi'_{j,j_3=j,\pm}$ is the eigenstate of $\not{D}'_{S^2}\sigma_3$ with the eigenvalue

$$\lambda = \pm\left(j + \frac{1}{2}\right). \tag{57}$$

Since J'_- commutes with $\not{D}'_{S^2}\sigma_3$, every descendant state

$$\chi'_{j,j_3,\pm} = (J'_-)^{j-j_3}(e^{i\phi}\sin\theta)^{j-\frac{1}{2}} \begin{pmatrix} \cos\frac{\theta}{2} \\ \mp\sin\frac{\theta}{2} \end{pmatrix} \tag{58}$$

shares the same eigenvalue (57). Namely, we have $(2j+1)$-fold degeneracy.

Thus we find the edge-localized eigenmode as

$$(\tilde{\psi}^E_{j,j_3,\pm})' \simeq \sqrt{\frac{m}{2}} \frac{e^{-m|r-r_0|}}{r} \begin{pmatrix} \chi'_{j,j_3,\pm} \\ \sigma_3\chi'_{j,j_3,\pm} \end{pmatrix}, \tag{59}$$

$$E \simeq \pm\frac{j+\frac{1}{2}}{r_0}. \tag{60}$$

The spectrum has a gap around $E = 0$, which is a bigger footprint of the gravity than that seen in the S^1 domain-wall case. The absence of the zero eigenvalue is consistent with the vanishing theorem [42], which states that the Dirac operator cannot have solutions on a manifold with non-negative curvature everywhere.

In fact, we can solve the Dirac equation in the original flat frame on $X = \mathbb{R}^3$ for finite m. We present the details in Appendix B. We just present the results below. The edge-localized

solutions are given by

$$\psi^{E>0}_{j,j_3,+} = \begin{cases} \frac{A}{\sqrt{r}} \begin{pmatrix} \sqrt{m^2-E^2} I_j(\sqrt{m^2-E^2}r)\chi_{j,j_3,+} \\ (m+E) I_{j+1}(\sqrt{m^2-E^2}r)\frac{\sigma\cdot x}{r}\chi_{j,j_3,+} \end{pmatrix} & (r<r_0) \\ \frac{B}{\sqrt{r}} \begin{pmatrix} (m+E) K_j(\sqrt{m^2-E^2}r)\chi_{j,j_3,+} \\ \sqrt{m^2-E^2} K_{j+1}(\sqrt{m^2-E^2}r)\frac{\sigma\cdot x}{r}\chi_{j,j_3,+} \end{pmatrix} & (r>r_0) \end{cases}, \tag{61}$$

and

$$\psi^{E<0}_{j,j_3,-} = \begin{cases} \frac{A'}{\sqrt{r}} \begin{pmatrix} (m-E) I_{j+1}(\sqrt{m^2-E^2}r)\chi_{j,j_3,-} \\ \sqrt{m^2-E^2} I_j(\sqrt{m^2-E^2}r)\frac{\sigma\cdot x}{r}\chi_{j,j_3,-} \end{pmatrix} & (r<r_0) \\ \frac{B'}{\sqrt{r}} \begin{pmatrix} \sqrt{m^2-E^2} K_{j+1}(\sqrt{m^2-E^2}r)\chi_{j,j_3,-} \\ (m-E) K_j(\sqrt{m^2-E^2}r)\frac{\sigma\cdot x}{r}\chi_{j,j_3,-} \end{pmatrix} & (r>r_0) \end{cases}, \tag{62}$$

where A, B, A', B', and E are determined by the continuity at $r = r_0$ and the normalization. The eigenvalue E is determined as a solution to

$$\frac{I_j}{I_{j+1}} \frac{K_{j+1}}{K_j}(\sqrt{m^2-|E|^2}r_0) = \frac{m+|E|}{m-|E|}. \tag{63}$$

It is a good exercise to confirm that the results are consistent with those in the $m \to \infty$ limit obtained in the rotated frame.

4.2. *Lattice analysis*

Let $(\mathbb{Z}/N\mathbb{Z})^3$ be a 3D lattice space and $0 \le \hat{x}, \hat{y}, \hat{z} \le N-1$ be the lattice coordinates. We impose the periodic boundary condition in every direction. We consider the Hermitian Wilson–Dirac operator as

$$H = \frac{1}{a}\gamma^5 \left(\sum_{i=1}^{3} \left[\gamma^i \frac{\nabla_i - \nabla_i^\dagger}{2} + \frac{1}{2}\nabla_i \nabla_i^\dagger \right] + \epsilon_A am \right), \tag{64}$$

where the region A inside the sphere is defined by

$$A = \left\{ (\hat{x},\hat{y},\hat{z}) \in (\mathbb{Z}/N\mathbb{Z})^3 \mid \left(\hat{x} - \frac{N-1}{2}\right)^2 + \left(\hat{y} - \frac{N-1}{2}\right)^2 + \left(\hat{z} - \frac{N-1}{2}\right)^2 < (\hat{r}_0)^2 \right\}, \tag{65}$$

and

$$\epsilon_A(\hat{x},\hat{y},\hat{z}) = \begin{cases} -1 & ((\hat{x},\hat{y},\hat{z}) \in A) \\ 1 & ((\hat{x},\hat{y},\hat{z}) \notin A) \end{cases} \tag{66}$$

is a step function that defines the S^2 domain-wall with the radius r_0. The center of the sphere is located at $(\frac{N-1}{2}, \frac{N-1}{2}, \frac{N-1}{2})$. Translating the center $(\frac{N-1}{2}, \frac{N-1}{2}, \frac{N-1}{2})$ to the origin, the chirality operator is defined by

$$\gamma_{\text{normal}} = \frac{\hat{x}}{\hat{r}}\gamma^1 + \frac{\hat{y}}{\hat{r}}\gamma^2 + \frac{\hat{z}}{\hat{r}}\gamma^3, \tag{67}$$

where $\hat{r}$ represents the length from the center of the circle. This operator is well defined only when N is even.

We solve the eigenvalue problem of H numerically. For the case with $ma = 0.875$, $r_0/a = 4$, and $N = 16$, we plot the eigenvalue spectrum in Fig. 7, where we arrange the eigenvalues in ascending order of j and the gradation represents their chirality.

We can see a good agreement between the numerical lattice data (circles) of Er_0 and the continuum results (crosses) between $-mr_0$ and mr_0, including the nontrivial degeneracy with

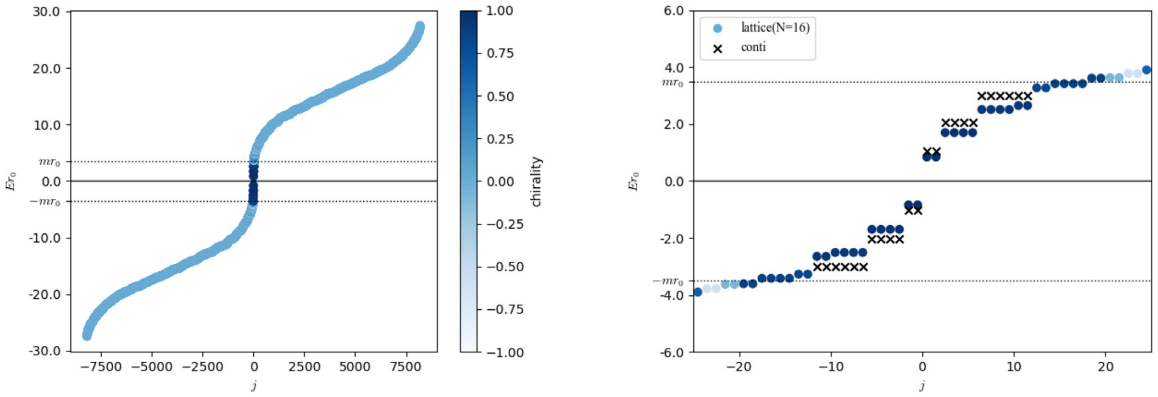

Fig. 7. The amplitude of the eigenfunction with $E_{\frac{1}{2}}$ at $ma = 0.875$, $r_0/a = 4$. In the left panel, the amplitude at every site in the whole 3D lattice is represented by the gradation, while it is given by the z-axis in the right panel focusing on the 2D plane at $\hat{z} = 7$.

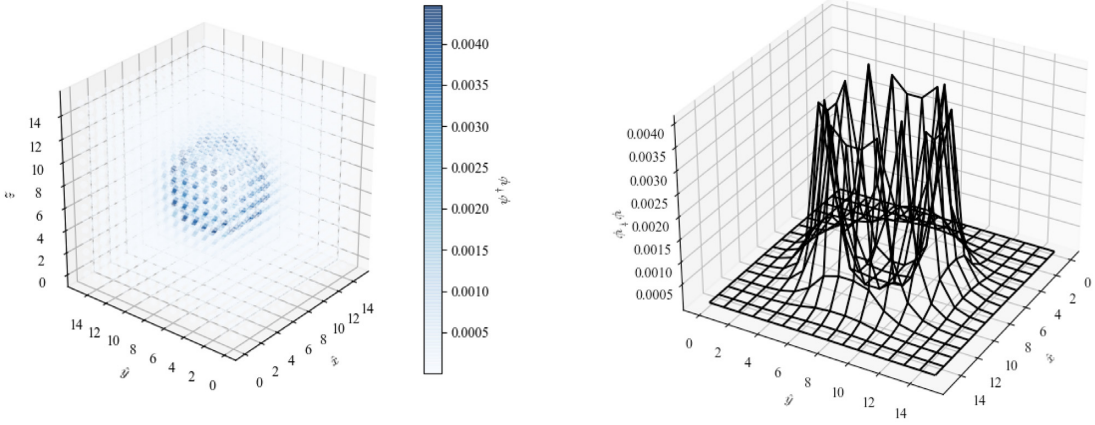

Fig. 8. The amplitude of the eigenfunction with $E_{\frac{1}{2}}$ at $ma = 0.875$ and $r_0/a = 4$. In the left panel, the amplitude at every site in the whole 3D lattice is represented by the gradation, while it is given by the z-axis in the right panel focusing on the 2D plane at $\hat{z} = 7$.

respect to the different value of j_3. It is also consistent with the continuum prediction that the chirality is almost unity. The gap from zero indicates that these modes feel gravity through the induced spin or spin^c connections. We notice that there are some chiral modes that do not have continuum counterparts near $E = m$. We expect that these modes will be absorbed into the bulk modes in the continuum limit when their continuum limit of the eigenvalues exceeds the mass. The near-zero modes are localized on the S^2 domain-wall as shown in Fig. 8, where the amplitude of the $E_{\frac{1}{2}}$ state is presented by the gradations.

Let us discuss the systematics due to the lattice spacing. In Fig. 9 we plot the deviation of $E_{\frac{1}{2}}$ with three masses $m = 10/L,\ 14/L,\ 20/L$ and $r_0 = L/4$ as in the previous section. The data show a linear dependence on the lattice spacing a to the continuum limit.

Next, we discuss the finite-volume effects. In Fig. 10 we plot the eigenvalue $E_{\frac{1}{2}} r_0$ at $r_0 = 4a$ and $ma = 0.875$ in the same way as in the previous section. A good convergence is seen after $N = L/a = 16 = 4r_0/a$.

The recovery of the rotational symmetry is also good. The smaller lattice spacing, the weaker the spiky shape becomes in Fig. 11. To quantify the rotational symmetry violation, we define

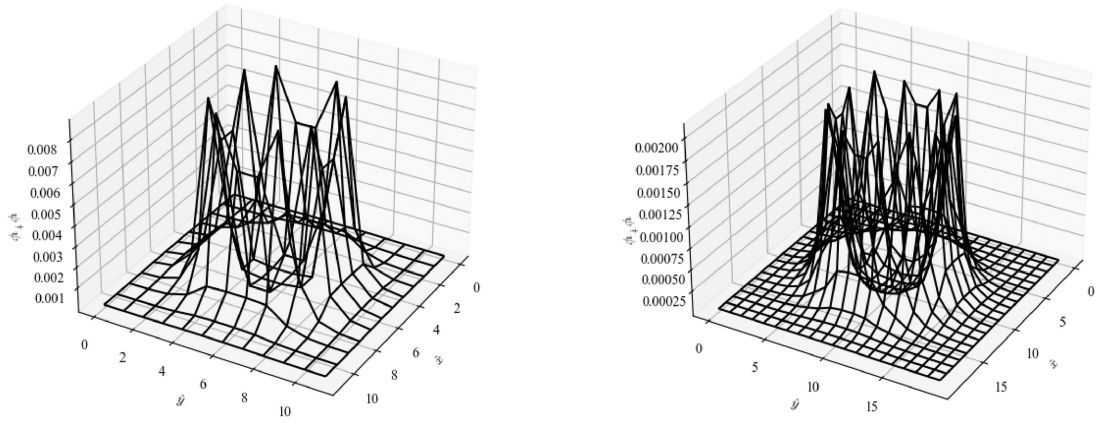

Fig. 9. The relative deviation of the eigenvalue is plotted as a function of the lattice spacing $a = \frac{1}{N}$.

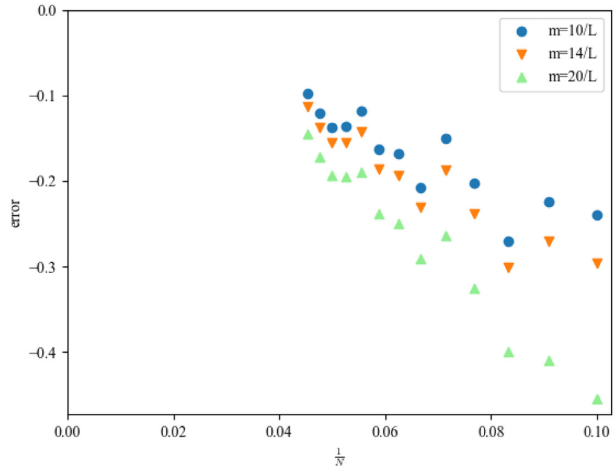

Fig. 10. Finite lattice size N scaling of the eigenvalue $E_{\frac{1}{2}} r_0$ at $ma = 0.875$ and $\hat{r}_0 = 4$.

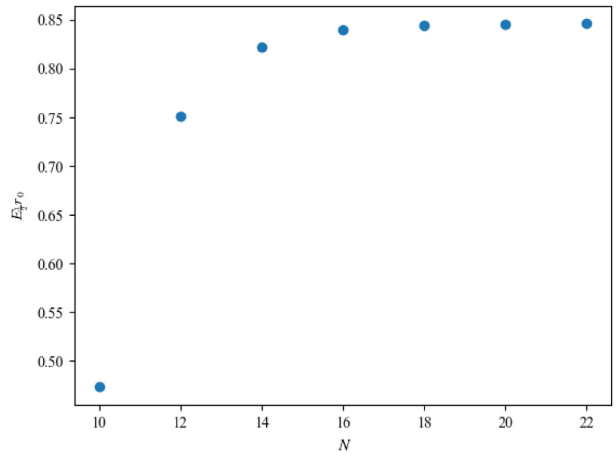

Fig. 11. The same plot as the right panel of Fig. 8 but with different lattice spacings $a = L/12$ (left) and $a = L/20$ (right).

Δ_{peak} as in the previous section but scan a 3D cube around the domain-wall. We plot the difference between the highest and lowest peaks in Fig. 12. Our data indicate automatic recovery

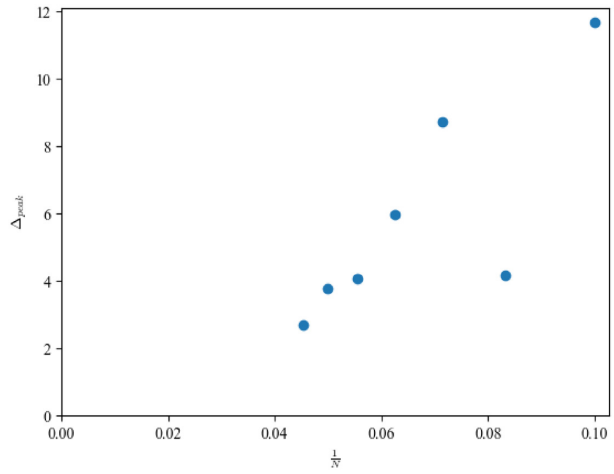

Fig. 12. The rotational symmetry violation measured by the difference between the highest and lowest peaks in the z-direction of the amplitude of the eigenfunction with $E_{\frac{1}{2}}$ ($m = 14/L$ and $r_0 = L/4$) among different x- and y-points covering the spherical domain-wall. See the main text for the details.

of the rotational symmetry, as is naively expected from its recovery of the higher-dimensional square lattice.

5. Summary and discussion

In this work, we have investigated fermion systems on a square lattice having a curved domain-wall mass term. On the S^1 domain-wall embedded into $\mathbb{R}^2$ and that of S^2 into $\mathbb{R}^3$, we have shown that the edge-localized modes appearing at the domain-wall feel gravity through the induced spin connection.

The effect of gravity or spin connections is encoded in the spectrum of the domain-wall fermion Dirac operators. In particular, we have found a gap from zero in the eigenvalues of the Dirac operator, which is consistent with the vanishing theorem [42], where the Dirac equation has no solution on a manifold with non-negative curvature everywhere.

For the cases of S^1 and S^2, we can analytically solve the continuum Dirac equation and compare the solutions with the lattice results. We have numerically solved the eigenproblem of the Hermitian lattice Dirac operator and found that the spectrum agrees well with that in the continuum theory. Our data at different lattice spacings indicate that the convergence to the continuum value is linear in a.

As expected, we have found that the near-zero eigenmodes of the Dirac operator are localized at the curved domain-walls. Although they have spiky shapes due to the rotational symmetry breaking, they monotonically become flat in the naive continuum extrapolation. This observation suggests that the rotational symmetry on the spheres is automatically recovered together with the simple classical continuum limit.

Our numerical analysis has been done on a lattice with periodic boundary conditions. The large volume extrapolation of the data indicates a good saturation when the lattice size is four times larger than the radius of the spherical domain-walls. The finite systematic is thus controlled in the same manner as in the conventional flat domain-wall fermion.

In this work, we have fixed the shape and location of the domain-walls. It is interesting to ask what happens when the domain-wall is allowed to move. On the lattice, the configuration of the domain-wall can be given by assigning ± 1 values to each lattice site. If we define the path

integral of these $\mathbb{Z}_2$ site valuables in such a way that its dynamics depends only on the effective curvature of the domain-walls, it may give a novel realization of quantum gravity coupled to the edge-localized chiral fermions.

In the examples given in this paper, we did not have zero eigenmodes of the effective Dirac operator with nonzero gravitational potentials. In these cases, the Atiyah–Singer index is trivially zero. In recent studies of the domain-wall fermions [19–22], the nontrivial Atiyah–Patodi–Singer index can be realized to describe the bulk and edge correspondence of anomaly inflow. Then a natural question is whether we can describe the gravitational anomaly inflow with curved domain-wall fermions, and describe the related index theorem on the lattice. A mixed anomaly with gauge link variables and gravity would also be interesting.

Acknowledgments

We thank M. Furuta, K. Hashimoto, M. Kawahira, S. Matsuo, T. Onogi, S. Yamaguchi, and M. Yamashita for useful discussions. This work was supported in part by JSPS KAKENHI Grant Numbers JP18H01216 and JP18H04484.

Funding

Open Access funding: SCOAP[3].

Appendix A. Weyl fermions on the domain-wall

In the literature, both in continuum theory [11,12] and on a lattice [13,14], the domain-wall fermion in odd dimensions has been employed to describe Weyl fermions. The Dirac operator in that case is

$$D = \not{D} + \epsilon m, \tag{A1}$$

which is not Hermitian. In the main text of this paper, we introduce two-flavor degrees of freedom to make a Hermitian Dirac operator. In this appendix, let us consider the single-flavor case.

Taking the frame decomposing the normal and tangent directions to the domain-wall, and the local scale transformation of the spinor field on $X = \mathbb{R}^n$: $\psi = \left(g^{IJ}\frac{\partial f}{\partial x^I}\frac{\partial f}{\partial x^J}\right)^{+\frac{1}{4}}\psi'$, the operator acts on ψ' as

$$D' = \underbrace{\gamma^a\left(e_a + \frac{1}{4}\sum_{bc}\omega_{bc,a}\gamma^b\gamma^c\right)}_{\tilde{\not{D}}} + \gamma^{n+1}\frac{\partial}{\partial t} + F + \epsilon m. \tag{A2}$$

In the large-m limit, the near-zero modes must converge to the edge-localized form

$$\psi' = e^{-m|t|}e^{-\int_0^t dt' F(y,t')}\chi_+, \tag{A3}$$

where χ_+ has the positive chirality of γ^{n+1}. The opposite chiral state appears for $D'^\dagger$. Thus, the Dirac operators D' and $D'^\dagger$ effectively act as $\tilde{\not{D}}_\pm = \tilde{\not{D}}\frac{1}{2}(1 \pm \gamma^{n+1})$, respectively, on the chiral edge modes. Thus, we have Weyl fermions as edge modes with a nontrivial spin connection induced by the curved domain-wall.

Appendix B. Direct computation of the edge modes

In this appendix, we solve the eigenproblem without taking the large-m limit in the original frame of $X = \mathbb{R}^3$. H is commutative with the following three operators:

$$J_i = 1 \otimes \hat{J}_i = 1 \otimes \left(L_i + \frac{1}{2}\sigma_i \right), \tag{B1}$$

$$J^2 = J_1^2 + J_2^2 + J_3^2 = 1 \otimes \hat{J}^2 \tag{B2}$$

$$P\psi(x) = (\sigma_3 \otimes 1)\psi(-x), \tag{B3}$$

where $L_i = -i\epsilon_{ijk}x^j\partial_k$ is an orbital angular momentum operator, $\hat{J}_i$ denotes the total angular momentum, and P is a parity operator. Therefore, let us label our two-component spinor $\chi_{j,j_3,\pm}$ by the eigenvalues of J^2, J_3, P:

$$\hat{J}^2\chi_{j,j_3,\pm} = j(j+1)\chi_{j,j_3,\pm} \tag{B4}$$

$$\hat{J}_3\chi_{j,j_3,\pm} = j_3\chi_{j,j_3,\pm} \tag{B5}$$

$$\chi_{j,j_3,\pm}(-x) = (-1)^{j\mp\frac{1}{2}}\chi_{j,j_3,\pm}(x) \tag{B6}$$

$$\chi_{j,j_3,-} = \frac{\sigma\cdot x}{r}\chi_{j,j_3,+}. \tag{B7}$$

Note that we can write them explicitly using spherical harmonics.

We obtain eigenstates with energy $E > 0$ as

$$\psi^{E>0}_{j,j_3,+} = \begin{cases} \frac{A}{\sqrt{r}}\begin{pmatrix} \sqrt{m^2-E^2}I_j(\sqrt{m^2-E^2}r)\chi_{j,j_3,+} \\ (m+E)I_{j+1}(\sqrt{m^2-E^2}r)\frac{\sigma\cdot x}{r}\chi_{j,j_3,+} \end{pmatrix} & (r < r_0) \\ \frac{B}{\sqrt{r}}\begin{pmatrix} (m+E)K_j(\sqrt{m^2-E^2}r)\chi_{j,j_3,+} \\ \sqrt{m^2-E^2}K_{j+1}(\sqrt{m^2-E^2}r)\frac{\sigma\cdot x}{r}\chi_{j,j_3,+} \end{pmatrix} & (r > r_0) \end{cases} \tag{B8}$$

and eigenstates with energy $E < 0$ as

$$\psi^{E<0}_{j,j_3,-} = \begin{cases} \frac{A'}{\sqrt{r}}\begin{pmatrix} (m-E)I_{j+1}(\sqrt{m^2-E^2}r)\chi_{j,j_3,-} \\ \sqrt{m^2-E^2}I_j(\sqrt{m^2-E^2}r)\frac{\sigma\cdot x}{r}\chi_{j,j_3,-} \end{pmatrix} & (r < r_0) \\ \frac{B'}{\sqrt{r}}\begin{pmatrix} \sqrt{m^2-E^2}K_{j+1}(\sqrt{m^2-E^2}r)\chi_{j,j_3,-} \\ (m-E)K_j(\sqrt{m^2-E^2}r)\frac{\sigma\cdot x}{r}\chi_{j,j_3,-} \end{pmatrix} & (r > r_0) \end{cases}, \tag{B9}$$

where A, B and A', B' are constants determined by the continuity at $r = r_0$ and the normalization. The eigenvalue E satisfies a solution to

$$\frac{I_j}{I_{j+1}}\frac{K_{j+1}}{K_j}(\sqrt{m^2-|E|^2}r_0) = \frac{m+|E|}{m-|E|}. \tag{B10}$$

Note that the sign of E corresponds to the eigenvalue of the parity operator P.

In the large-mass limit or $m \gg E$, the energy converges to

$$E \simeq \pm\frac{j+\frac{1}{2}}{r_0}, \ \left(j = \frac{1}{2}, \frac{3}{2}\cdots \right), \tag{B11}$$

where $\pm$ corresponds to the eigenvalue $(-1)^{j\mp\frac{1}{2}}$ of P. We can see the gap from zero as a gravitational effect.

The normalized eigenstate in that limit is obtained as

$$\tilde{\psi}^{E}_{j,j_3,\pm} \simeq \sqrt{\frac{m}{2}}\frac{e^{-m|r-r_0|}}{r}\begin{pmatrix} \chi_{j,j_3,\pm} \\ \frac{\sigma\cdot x}{r}\chi_{j,j_3,\pm} \end{pmatrix}, \tag{B12}$$

which is an eigenstate of the gamma matrix

$$\gamma_{\text{normal}} := \sum_{i=1}^{3} \frac{x^i}{r} \gamma^i \tag{B13}$$

facing to the normal direction of S^2, and it has an eigenvalue $+1$.

References

[1] H. W. Hamberl Gen. Relat. Gravit. **41**, 817 (2009).
[2] T. Regge, Nuovo Cimento **19**, 558 (1961).
[3] R. C. Brower, G. Fleming, A. Gasbarro, T. Raben, C.-I. Tan, and E. Weinberg, PoS **LATTICE2015**, 296 (2016), [arXiv:1601.01367 [hep-lat]] [Search inSPIRE].
[4] J. Ambjorn, J. Jurkiewicz, and R. Loll, Nucl. Phys. B **610**, 347 (2001) [arXiv:hep-th/0105267] [Search inSPIRE].
[5] R. C. Brower, E. S. Weinberg, G. T. Fleming, A. D. Gasbarro, T. G. Raben, and C.-I. Tan, Phys. Rev. D **95**, 114510 (2017) [arXiv:1610.08587 [hep-lat]] [Search inSPIRE].
[6] S. Catterall, J. Laiho, and J. Unmuth-Yockey, J. High Energy Phys. **1810**, 013 (2018) [arXiv:1806.07845 [hep-lat]] [Search inSPIRE].
[7] J. Ambjorn, J. Gizbert-Studnicki, A. Görlich, and D. Németh, J. High Energy Phys. **04**, 103 2022, [arXiv:2202.07392 [hep-lat]] [Search inSPIRE].
[8] R. C. Brower, M. Cheng, and G. T. Fleming, PoS **LATTICE2014**, 318 (2015).
[9] J. Nash, Ann. Math. **63**, 20 (1956).
[10] M. L. Gromov and V. A. Rokhlin, Russ. Math. Surv. **25**, 1 (1970).
[11] R. Jackiw and C. Rebbi, Phys. Rev. D **13**, 3398 (1976).
[12] C. G. Callan Jr and J. A. Harvey, Nucl. Phys. B **250**, 427 (1985).
[13] D. B. Kaplan, Phys. Lett. B **288**, 342 (1992).
[14] Y. Shamir, Nucl. Phys. B **406**, 90 (1993) [arXiv:hep-lat/9303005] [Search inSPIRE].
[15] V. Furman and Y. Shamir, Nucl. Phys. B **439**, 54 (1995) [arXiv:hep-lat/9405004] [Search inSPIRE].
[16] P. H. Ginsparg and K. G. Wilson, Phys. Rev. D **25**, 2649 (1982).
[17] M. Luscher, Phys. Lett. B **428**, 342 (1998) [arXiv:hep-lat/9802011] [Search inSPIRE].
[18] P. Hasenfratz, V. Laliena, and F. Niedermayer, Phys. Lett. B **427**, 125 (1998) [arXiv:hep-lat/9801021] [Search inSPIRE].
[19] H. Fukaya, T. Onogi, and S. Yamaguchi, Phys. Rev. D **96**, 125004 (2017) [arXiv:1710.03379 [hep-th]] [Search inSPIRE].
[20] H. Fukaya, M. Furuta, S. Matsuo, T. Onogi, S. Yamaguchi, and M. Yamashita, PoS **LATTICE2019**, 061 (2019) [arXiv:2001.01428 [hep-lat]] [Search inSPIRE].
[21] H. Fukaya, M. Furuta, Y. Matsuki, S. Matsuo, T. Onogi, S. Yamaguchi, and M. Yamashita, 38th Int. Symp. Lattice Field Theory[arXiv:2111.11040 [hep-th]] [Search inSPIRE].
[22] H. Fukaya, N. Kawai, Y. Matsuki, M. Mori, K. Nakayama, T. Onogi, and S. Yamaguchi, Prog. Theor. Exp. Phys. **2020**, 043B04 (2020) [arXiv:1910.09675 [hep-lat]] [Search inSPIRE].
[23] H. Jensen and H. Koppe, Ann. Phys. **63**, 586 (1971).
[24] R. C. T. da Costa, Phys. Rev. A **23**, 1982 (1981).
[25] Y. V. Pershin and C. Piermarocchi, Phys. Rev. B **72**, 125348 (2005).
[26] G. Ferrari and G. Cuoghi, Phys. Rev. Lett. **100**, 230403 (2008).
[27] F. T. Brandt and J. A. Sánchez-Monroy, Phys. Lett. A **380**, 3036 (2016).
[28] S. Matsutani and H. Tsuru, Phys. Rev. A **46**, 1144 (1992).
[29] S. Matsutani, Prog. Theor. Phys. **91**, 1005 (1994).
[30] S. Matsutani, J. Phys. A: Math. Gen. **30**, 4019 (1997).
[31] M. Burgess and B. Jensen, Phys. Rev. A **48**, 1861 (1993).
[32] A. Szameit, F. Dreisow, M. Heinrich, R. Keil, S. Nolte, A. Tünnermann, and S. Longhi, Phys. Rev. Lett. **104**, 150403 (2010).
[33] J. Onoe, T. Ito, H. Shima, H. Yoshioka, and S. I. Kimura, EPL **98**, 27001 (2012).
[34] D.-H. Lee, Phys. Rev. Lett. **103**, (2009).
[35] K.-I. Imura, Y. Yoshimura, Y. Takane, and T. Fukui, Phys. Rev. B **86**, 235119 (2012).

[36] V. Parente, P. Lucignano, P. Vitale, A. Tagliacozzo, and F. Guinea, Phys. Rev. B **83**, 075424 (2011) [arXiv:1011.0565 [cond-mat.mes-hall]] [Search inSPIRE].
[37] Y. Takane and K.-I. Imura, J. Phys. Soc. Jpn **82**, 074712 (2013) [arXiv:1303.2179 [cond-mat.mes-hall]] [Search inSPIRE].
[38] S. Catterall and A. Pradhan, (2022), [arXiv:2201.00750 [hep-th]] [Search inSPIRE].
[39] N. Butt, S. Catterall, A. Pradhan, and G. C. Toga, Phys. Rev. D **104**, 094504 (2021) [arXiv:2101.01026 [hep-th]] [Search inSPIRE].
[40] S. Aoki and H. Fukaya, PoS **LATTICE2021**, 535 (2022), [arXiv:2111.11649 [hep-lat]] [Search in SPIRE].
[41] A. A. Abrikosov, Jr, (2002), [arXiv:hep-th/0212134][Search inSPIRE].
[42] Th. Friedrich, Math. Nachr. **97**, 117 (1980).